JACS
JOURNAL OF THE AMERICAN CHEMICAL SOCIETY

Article

pubs.acs.org/JACS

Versatile *de Novo* Enzyme Activity in Capsid Proteins from an Engineered M13 Bacteriophage Library

John P. Casey, Jr.,[†] Roberto J. Barbero,[†] Nimrod Heldman,[‡] and Angela M. Belcher*[,†,‡,§]

[†]Biological Engineering, [‡]Materials Science and Engineering, and [§]Koch Institute for Integrative Cancer Research, Massachusetts Institute of Technology, 77 Massachusetts Avenue, 76-561, Cambridge, Massachusetts 02139, United States

Supporting Information

ABSTRACT: Biocatalysis has grown rapidly in recent decades as a solution to the evolving demands of industrial chemical processes. Mounting environmental pressures and shifting supply chains underscore the need for novel chemical activities, while rapid biotechnological progress has greatly increased the utility of enzymatic methods. Enzymes, though capable of high catalytic efficiency and remarkable reaction selectivity, still suffer from relative instability, high costs of scaling, and functional inflexibility. Herein, we developed a biochemical platform for engineering *de novo* semisynthetic enzymes, functionally modular and widely stable, based on the M13 bacteriophage. The hydrolytic bacteriophage described in this paper catalyzes a range of carboxylic esters, is active from 25 to 80 °C, and demonstrates greater efficiency in DMSO than in water. The platform complements biocatalysts with characteristics of heterogeneous catalysis, yielding high-surface area, thermostable biochemical structures readily adaptable to reactions in myriad solvents. As the viral structure ensures semisynthetic enzymes remain linked to the genetic sequences responsible for catalysis, future work will tailor the biocatalysts to high-demand synthetic processes by evolving new activities, utilizing high-throughput screening technology and harnessing M13's multifunctionality.

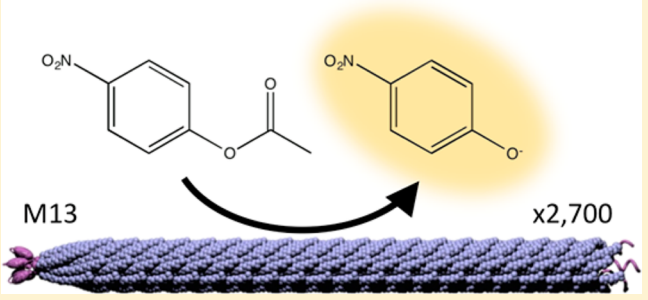

INTRODUCTION

Enzymes and biocatalysts potentiate a wide range of chemical activities and functionality not practical with abiotic processes. Performance enhancements in substrate specificity, reaction selectivity, and catalytic efficiency drive their accelerating implementation in reactions that have traditionally employed inorganic catalysts, such as the chiral resolution of alcohols and the oxidation of alkane precursors.[1−3] Enzymes can result in lower process temperatures for industrial reactions while decreasing the amount of solvent and waste, reducing energy and material costs.[4] Additionally, the unique geometries and energy states created by enzyme active sites allow for the generation of many important chemicals with no effective inorganic means of production (for example, artemisinin[5] and carotenoids[6]). The inherent modularity of biomolecules complements such advantages by promising engineers more control over enzyme outputs. Not only is protein structure manipulable by genetic means, but well-characterized biochemical functional handles allow for catalytically significant post-translational modifications. As successful examples of enzymatic approaches proliferate,[7−9] however, challenges remain in adapting proteins to alternate environs or functions.[10] Native enzymes often exhibit short lifetimes, on the scale of hours without modification or immobilization;[11] outside of native pH and temperature, their functionality can become less predictable. Similarly, while some enzymes have been found to have novel activity or even greater thermostability in organic solvents,[3,12] they often become substantially less active when removed from aqueous conditions.[13]

Fortunately, functional tools to engineer and adapt enzymes have advanced considerably in recent years. Attempts to overcome traditional biocatalytic limitations usually fall into one of two strategies: modifying pre-existing enzymes by rational engineering or directed evolution, or the generation and development of *de novo* catalytic entities. The former has a longer history and can include targeted mutations to, for instance, improve protein lifetime via insertion of disulfide linkages.[14] Immobilization techniques have been especially successful in improving temporal and thermal stability and have been implemented broadly for the industrial production of pharmaceuticals and a number of other common chemicals (for review, see Zhou and Hartmann[15] or Bommarius and Paye[16]). Chemical and genetic modifications, as well as myriad cross-linking strategies, have also been successful in modulating stability and selectivity.[17] Directed evolution approaches have made notable contributions by sampling larger windows of the functional landscape to identify unintuitive active site modifications[7,18−20] (see Turner[21] for recent review). This strategy has been implemented in a variety of processes, including Lipitor production and the manufacture of chiral amines.[10] While the engineering of existing enzymes has been

Received: June 24, 2014
Published: October 24, 2014

   dx.doi.org/10.1021/ja506346f | J. Am. Chem. Soc. 2014, 136, 16508−16514

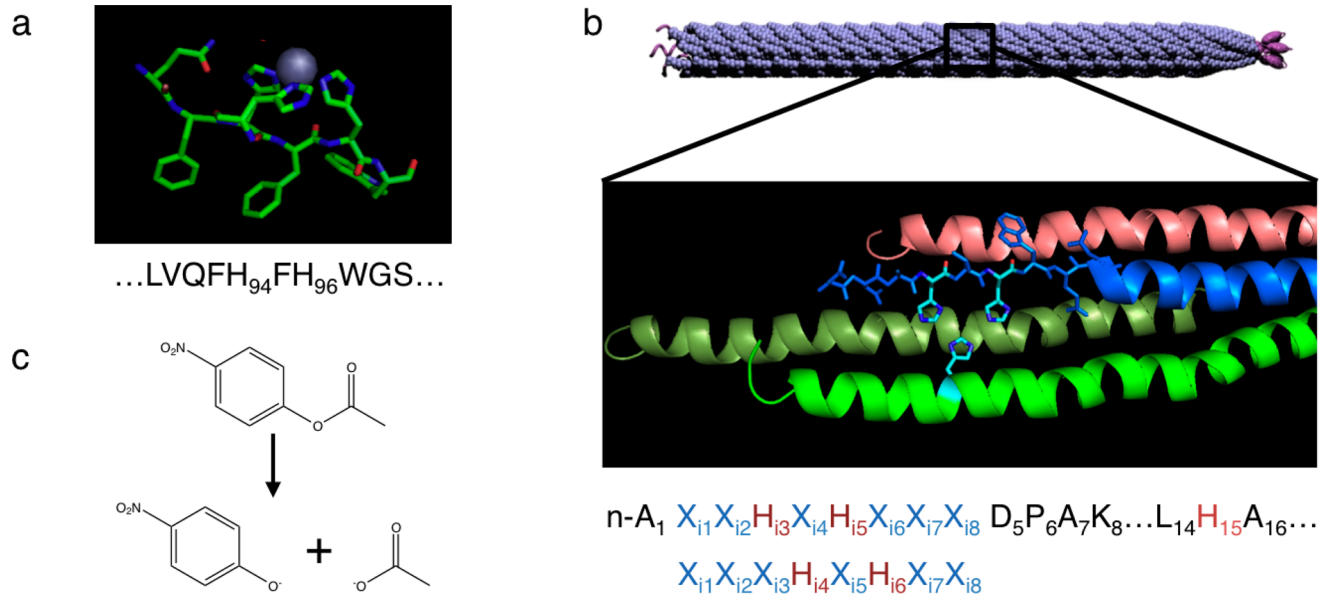

Figure 1. Design of semisynthetic active sites for hydrolysis. (a) The active site of bCAII consists of three histidine residues coordinating a Zn^{2+} ion (1CA2[40]). The front-most His residue shown comes from an adjacent β-sheet. (b) The cloning strategy involved mutating three specific residues on M13 pVIII to histidine (red, sequence at bottom) and randomizing adjacent terminal residues (blue). His pairs were at i3,i5 or i4,i6; backbone mutations were at S13, Q15, G23, or A27. Image includes PDB file 2C0W.[39] (c) The hydrolysis of *p*-nitrophenyl acetate (pNPA) yields colorimetric *p*-nitrophenylate (pNP), which can be detected via absorbance at 400 nm, and acetate.

increasingly successful in improving those enzymes and, in some cases, adapting them to tangential or novel reactions,[22,23] such approaches are rarely fully generalizable. An alternate strategy involves co-opting structural domains of unrelated proteins for *de novo* active sites or designing new protein structures entirely. By sampling completely independent domains of the fitness landscape, such undertakings allow for unique combinations of targeted functional attributes, especially when function can be uncoupled from structural stability.[24] By building protein domains from the bottom up, one increases the potential for diverse activity.[25,26] Three- and four-helix bundles have been utilized for redox,[27−29] peroxidase,[30] carbonic anhydrase,[31] esterase,[32] and lipase activity.[33] Computational design and the insertion of exogenous active sites into existing proteins have led to similarly successful outcomes.[34−36] Such varied approaches are rapidly broadening the scope of biocatalysts in their activity and applications.

Previous *de novo* engineered enzymes have recapitulated target enzymatic activity to a remarkable degree, but few have been developed for the variety of non-native environments common to industrial processes. Here, we sought to develop a robust, versatile biocatalytic platform potentiating the catalysis of targeted reactions in nonstandard environments. To do so, we fused multiple above-mentioned strategies, recreating active site geometry from a highly efficient enzyme on an otherwise entirely structural protein assembly and selecting a functional clone. As a template, M13 bacteriophage was chosen for its excellent thermostability, scalability, multivalency, and ease of genetic modification. M13 is a filamentous macromolecule 880 nm in length and 6.5 nm in diameter, with 2700 identical pVIII capsid proteins wrapping 7 kbp of single-stranded DNA. By displaying catalytic motifs from the well-studied carbonic anhydrase enzyme on the major coat protein, pVIII, we endowed M13 with thousands of semisynthetic enzymes capable of catalyzing hydrolysis reactions. With a relatively open binding pocket, the M13 constructs exhibited diverse activity, catalyzing a range of substrates less accessible to native carbonic anhydrase. Moreover, the catalytic efficiency increased substantially outside of aqueous reaction conditions and at elevated temperatures, wherein the wild-type enzyme became inactive. Thus, interfacing biochemical functions with non-biological conditions, M13 semisynthetic enzymes inform continuing studies of protein design while opening new opportunities in sustainable molecular biocatalysis.

RESULTS

Building M13 Bacteriophage Libraries with Incorporated Catalytic Motifs. In order to design effective biocatalysts, we leveraged our lab's experience engineering M13 against the extensive literature on carbonic anhydrase enzymes to build a set of pVIII libraries incorporating catalytic motifs found in anhydrase active sites. Of the five M13 coat proteins, pIII is the largest and most commonly engineered; indeed, previous work has successfully cloned full anhydrase enzymes into M13 pIII.[37] However, for this work we chose instead to modify the 50 amino acid (AA) pVIII protein for a more multivalent (2700 copies vs $\leq$5 for pIII) and durable semisynthetic enzyme system. In addition to outnumbering the minor coat proteins by >500-fold, pVIII's simple, symmetrically repeated α-helices are highly stable to environmental extremes. Fiber diffraction experiments of filamentous bacteriophage have detailed the position and orientation of these proteins relative to each other (PDB 1IFJ[38] and PDB 2C0W[39]). Such information makes the pVIII of M13 particularly tractable for biological engineers, allowing one to rationally replace native residues to approximate active site geometries and chemistries while interrogating primary structure relationships.

In doing so, we chose to model our pVIII constructs after carbonic anhydrase II (CAII), a thoroughly characterized and highly efficient zinc-based metalloenzyme (Figure 1a) (PDB 1CA2).[40] CAII's active site has two histidine residues separated by phenylalanine in an α-helix and a third histidine residue in a

dx.doi.org/10.1021/ja506346f | J. Am. Chem. Soc. 2014, 136, 16508−16514

proximal β-sheet; the three His residues together bind a Zn^{2+} ion whose fourth coordination site is occupied by a hydroxyl ion or substrate. To replicate this geometry, we built a library of plasmids encoding a pair of His residues at fixed positions, surrounded by randomized amino acids, in 8 AA inserts located at the surface-exposed N-terminus of pVIII (Figure 1b; see Supplementary Figure 1 in the Supplementary Results for more details on the oligonucleotide libraries). A third histidine ("backbone" histidine) was inserted deeper into the pVIII (further from the N-terminus), such that each N-terminal pair of histidine residues on a pVIII would be in close proximity to the backbone histidine of an adjacent pVIII protein. Since the 8 AA inserts are likely not part of the backbone α-helix, which is believed to be broken by Pro6, the specific orientation of the eight residues within each hypothetical insert is not readily inferable. We generated an ensemble of M13 libraries with two variables: the position of the histidine pair in the N-terminus and the location of the backbone histidine, seeking to maximize the potential for ion coordination between three His residues on adjacent helices. PDB files 1CA2 for CAII and 2C0W for M13 were used for evaluation. Our analyses of the structural models indicated that the most favorable trios involved pairs i3,i5 and i4,i6 on the insert (positions along the 8 AA peptide insert will be indicated with an 'i' prefix; the other positions will retain wild-type numbering with no prefix) complemented with backbone histidines at the 13th, 15th, 23rd, or 27th residue from the native N-terminus. Supporting these selections, the positions match closely with those residues downstream of the N-terminus expected to be most surface exposed in wild-type models.[38]

Individual clones from these libraries were then surveyed for primary sequence similarity to the CAII active site residues, with an emphasis on hydrophobicity in the immediate vicinity of the coordinating histidines. A subpopulation of 10 sequences was selected for initial experimental characterization, and subsequently the clone DDAHVHWE, G23H (DDAH) was chosen for further study (Supplementary Figure 2).

Clone DDAH Catalyzes the Aqueous Hydrolysis of *p*-Nitrophenyl Acetate. In order to characterize the bacteriophage-displayed semisynthetic enzymes, we measured hydrolysis of nitrophenyl esters (Figure 1c). *p*-Nitrophenyl acetate (pNPA) hydrolysis is well-characterized as a model reaction for CAII,[37,41] rationally engineered enzymes,[42] *de novo* peptides,[31,33,43] and novel materials.[44] From the subpopulation of bacteriophage clones we tested, the clone DDAH was determined to be the most reliable and consistent candidate (Supplementary Figure 2) and was chosen for further characterization. In ion coordination studies, the clone was found to bind Zn^{2+} with a K_D of 6 μM via microscale thermophoresis (Supplementary Figure 3); reactions were then performed with 25 μM $ZnSO_4$.

The hydrolysis activity of the bacteriophage was quantified by the catalytic efficiency, k_{cat}/K_M, according to Michaelis–Menten kinetics (see Supplementary Methods):

$$\frac{d[P]}{dt} = \frac{k_{cat}[E][S]}{K_M + [S]}$$

Each pVIII protein was considered conservatively to be one active site, so that each bacteriophage represented 2700 catalytic sites. As such, clone DDAH was found to hydrolyze pNPA with k_{cat}/K_M = 0.535 M^{-1} s^{-1} for each pVIII subunit (Figure 2 and Supplementary Table 1) in PBS at pH 7.4; by

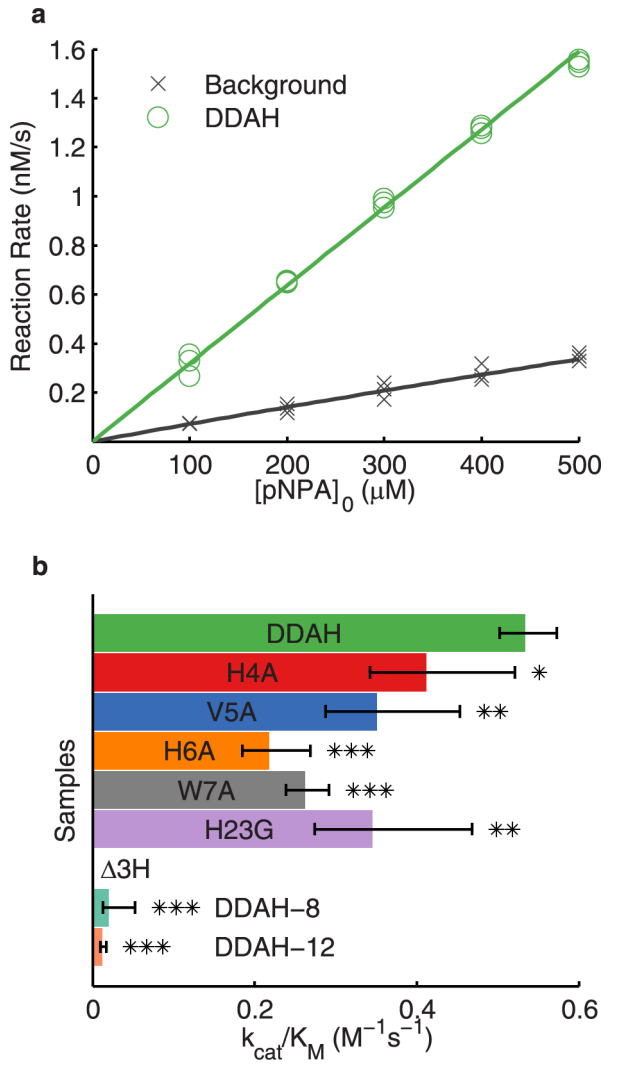

Figure 2. M13 clone DDAH catalyzes the aqueous hydrolysis of pNPA. (a) Plot of hydrolysis rate vs substrate concentration for M13 clone DDAH (green circles) and the control reaction (PBS, gray ×'s). (b) Respective k_{cat}/K_M catalytic rates for DDAH and a number of mutants. Δ3H: terminal two histidines mutated to alanine and third histidine returned to glycine (as wild-type); DDAH-8 and DDAH-12: 8-mer and 12-mer synthetic peptides, respectively, comprised of the terminal peptide sequence of DDAH pVIII. Error bars represent 95% confidence intervals for values fit by Lineweaver–Burk analysis. *p*-values: * <0.05; ** <0.005; *** < 0.0005; represents two-sample *t* test for regressed coefficients of DDAH and given sample.

comparison, wild-type bovine carbonic anhydrase (bCAII, Worthington Biochemical Corporation #LS001260) hydrolyzed pNPA at a rate of 194 M^{-1} s^{-1} and solubilized L-His monomers measured 0.021 M^{-1} s^{-1}. The activity of DDAH thus represents a significant coordination between the residues, while remaining far lower than that of the wild-type enzyme. The inferred k_{cat}, 0.002 and 1.2 s^{-1} for DDAH and bCAII, respectively, implies that a difference in turnover rate is a far larger contributing factor than substrate binding, though the k_{cat} values themselves are less precise calculations from our Lineweaver–Burk plots than k_{cat}/K_M. We believe the low activity compared to carbonic anhydrase is in part related to the conformational flexibility of the pVIII termini in aqueous solutions; the 10 terminal residues following P_6 likely lack secondary structure. This hypothesis is considered in more

dx.doi.org/10.1021/ja506346f | J. Am. Chem. Soc. 2014, 136, 16508–16514

detail in the Discussion section. Additionally, the current strategy did not target second-shell interactions between nearby AA residues and the inserted zinc-coordinating histidines; such interactions play a large role in catalytic efficiency and their inclusion would likely improve the construct's activity.

To more thoroughly understand the contributing factors of the DDAH active site, we performed an alanine scan on the peptide insert and engineered two additional histidine substitutions: DDAH with the His residue at position 23 mutated H23G, as in wild-type M13, and a Δ3H clone engineered with H4A, H6A, and H23G mutations so that no histidine residues remain. The results are summarized in Figure 2b and Supplementary Table 1. Each mutant's catalytic activity was significantly lower than the original DDAH clone (two-sample p-value <0.05), though all but the Δ3H clone had measurable hydrolysis activity above background. Notably, the tryptophan residue in the insert, at the same position relative to the histidine pair as in CAII (FHFHW, Figure 1a), was found to be important for hydrolysis activity. In addition to the M13 mutants, we tested free-floating synthetic peptides representing the N-terminal 8 and 12 AAs; that is, DDAHVHWE and DDAHVHWEDPAK, not expressed on the surface of M13. These peptides showed negligible activity (0.021 and 0.013 M^{-1} s^{-1}, respectively).

DDAH Activity Is Robust in Nonaqueous Solvents. As many synthetic processes involve harsh, abiotic environments,[2] we sought to determine the catalytic efficiency of DDAH in relevant nonaqueous solvents. The substrate has excellent solubility and stability in DMSO, a highly useful solvent in, for instance, pharmaceuticals production,[45] so this solvent was chosen for further investigation. DDAH exhibited a 30-fold increase in catalytic efficiency in 98% DMSO, wherein k_{cat}/K_M = 16.87 M^{-1} s^{-1}, while background levels remained roughly the same (Supplementary Table 2). The activity is stable for hours, through the length of the experiments run (Figure 3). The phage assemblies reach a steady-state k_{cat} and K_M within 40 min of mixing, and the overall k_{cat}/K_M shows no significant difference throughout the experiment. The DDAH clone itself is rendered noninfectious after exposure to DMSO (Supplementary Table 3), indicating that pIII is irreversibly denatured, even though the overall filamentous structure remains intact (see transmission electron micrographs, Supplementary Figure 4). Wild-type bCAII showed no measurable activity in DMSO (at 67 nM, Figure 4a). Similarly, another M13 clone with activity in PBS, TENM (TENMHGTM, 23H; Supplementary Figure 2), exhibited no activity in DMSO.

DDAH Catalyzes a Range of Substrates. A critical feature of the M13 semisynthetic enzyme design is the openness of the active site, situated between the most N-terminal nine amino acids of pVIII and an adjacent pVIII α helix; the active site is relatively unimpeded. We therefore sought to characterize the activity of DDAH with respect to substrates with increasing carbon chain length, pNPA (n = 2), p-nitrophenyl propionate (pNPP, n = 3), p-nitrophenyl butyrate (pNPB, n = 4), and p-nitrophenyl palmitate (pNPPa, n = 15, lipase substrate) (Figure 4b). Only pNPA and pNPB were soluble in the aqueous reaction mixture, but the stability of DDAH in DMSO enabled us to study substrates not soluble in PBS. Solubilized L-histidine was used as a control, as it catalyzes ester hydrolysis at a measurable level and because histidine residues are critical for the aqueous activity of DDAH clones (Figure 2b). In aqueous reactions, DDAH hydrolyzed pNPB at just over half the efficiency of pNPA, with k_{cat}/K_M =

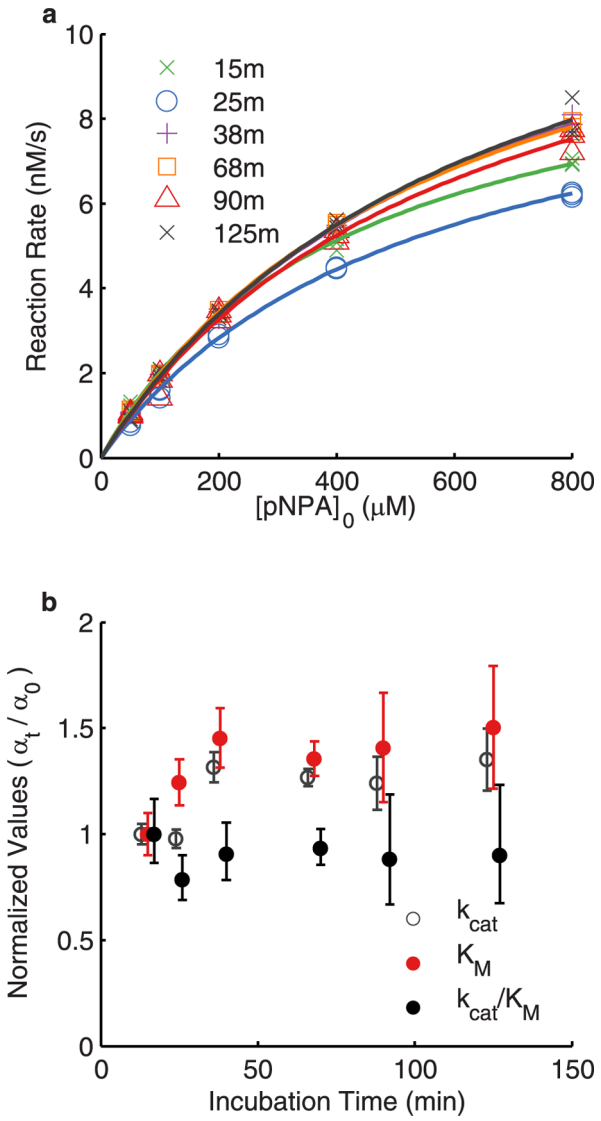

Figure 3. DDAH stably catalyzes pNPA hydrolysis in DMSO. (a) Hydrolysis rate of pNPA vs substrate concentration for DDAH clones solubilized in DMSO for different lengths of time (markers), with regressions (lines). (b) k_{cat}/K_M values through 2 h in DMSO stay ~90% of the initial value. Catalytic parameters (α_t) are determined from a NLLS fit to the Michaelis–Menten equation and normalized to their t_0 = 15 min values (α_0, earliest time point to mix and plate out samples with substrate). Time points: 15, 25, 38, 68, 90, and 125 min. Error bars are 95% confidence intervals for k_{cat} and K_M, 90% confidence intervals for k_{cat}/K_M (0.95^2).

0.282 M^{-1} s^{-1} (Figure 4c). By comparison, wild-type carbonic anhydrase has been found to catalyze pNPB hydrolysis with only 2% the activity with which it hydrolyzes pNPA.[42] The nonaqueous reactions, again, were catalyzed far faster than the water-based reactions. In 98% DMSO, the k_{cat}/K_M = 16.87 M^{-1} s^{-1} for DDAH-catalyzed hydrolysis of pNPA dropped to 8.92 M^{-1} s^{-1} for pNPP (Figure 4d). Notably, DDAH catalyzed the lipase substrate pNPPa with a catalytic efficiency 5.89 M^{-1} s^{-1}, which is 35% of the catalytic efficiency of DDAH with the much smaller substrate pNPA. The capacity to react with substrates of such varying size makes DDAH a promising alternative to biocatalysts whose substrate versatility is limited by steric hindrance. Interestingly, despite no demonstrable activity in aqueous reactions and no histidines on pVIII, the

dx.doi.org/10.1021/ja506346f | J. Am. Chem. Soc. 2014, 136, 16508–16514

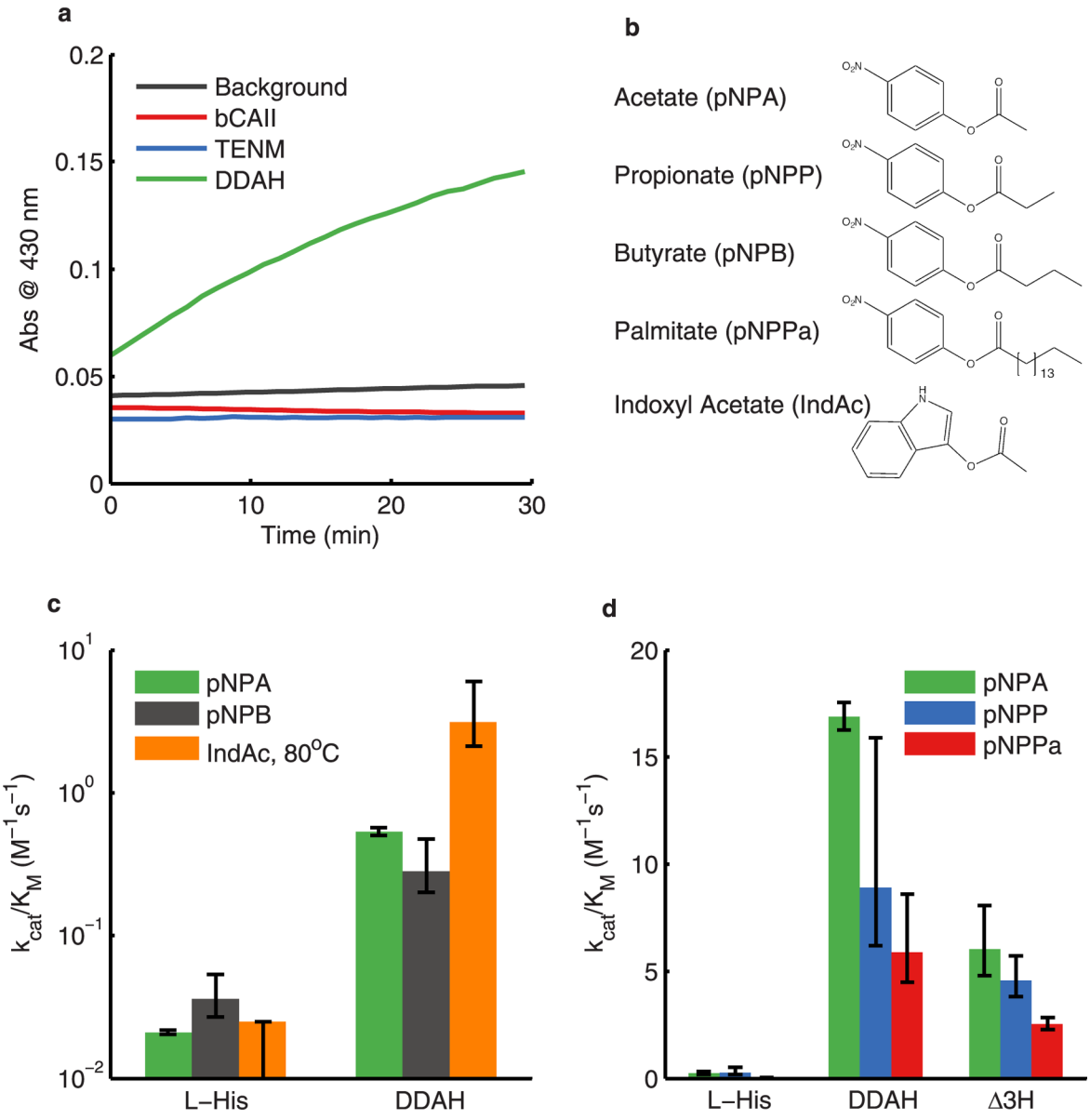

Figure 4. DDAH demonstrates versatile catalytic activity in water and DMSO. (a) Typical product accumulation vs time plot in 98% DMSO; wild-type bCAII and TENM (a control M13 phage clone with two histidine substitutions) exhibit no measurable hydrolysis activity. $[pNPA]_0 = 250\ \mu M$. (b) Structures of the five hydrolysis substrates. (c) Log−scale plot of L-histidine and DDAH in the aqueous (98% PBS) hydrolysis of nitrophenyl esters at room temperature and indoxyl acetate at 80 °C. (d) Catalytic efficiency of L-histidine, DDAH, and Δ3H solubilized in a 98% DMSO reaction mixture with substrates of differing carbon chain lengths. Error bars in (c and d) represent 95% confidence intervals for values fit by Lineweaver−Burk analysis. In (c), IndAc hydrolysis by L-histidine indistinguishable from background rate; Lineweaver−Burk upper error bar not available.

Δ3H clone was catalytically active in the DMSO reaction mixture (Figure 4d). While not as efficient a catalyst as DDAH clone, the activity of this mutant is intriguing and may be a result of remaining exposed aspartates (three) and glutamates (one).

In addition to larger nitrophenyl esters, we assayed the activity of DDAH toward a less active carboxylic ester, indoxyl acetate (IndAc). Upon hydrolysis of the acetate moiety, indoxyl is rapidly converted to indigo in the presence of oxygen. Though insoluble in water, indigo production could be quantified upon dilution into DMSO. We were able to detect no activity at room temperature. However, at 80 °C DDAH hydrolyzed the substrate with $k_{cat}/K_M = 3.13\ M^{-1}\ s^{-1}$. This compares with 30.47 $M^{-1}\ s^{-1}$ for bCAII, while the activity of solubilized L-histidine measured 0.025 $M^{-1}\ s^{-1}$ and was statistically indistinguishable from background hydrolysis.

Catalytic Efficiency Increases with Higher Temperatures. In order to characterize the effect of temperature on DDAH activity, pNPA hydrolysis was measured under heated conditions. Many industrial processes are conducted at raised temperatures, both to improve catalytic performance and to limit bacterial contamination.[46] Accordingly, pNPA hydrolysis experiments were conducted in DMSO at 40 and 65 °C, with the latter representing a temperature at which bacterial growth is unlikely. Regressed catalytic parameters are shown in Figure 5, normalized to values at room temperature to facilitate comparison. The DDAH catalytic rate k_{cat} increased significantly for the heated reactions, while the constant K_M remained

dx.doi.org/10.1021/ja506346f | J. Am. Chem. Soc. 2014, 136, 16508−16514

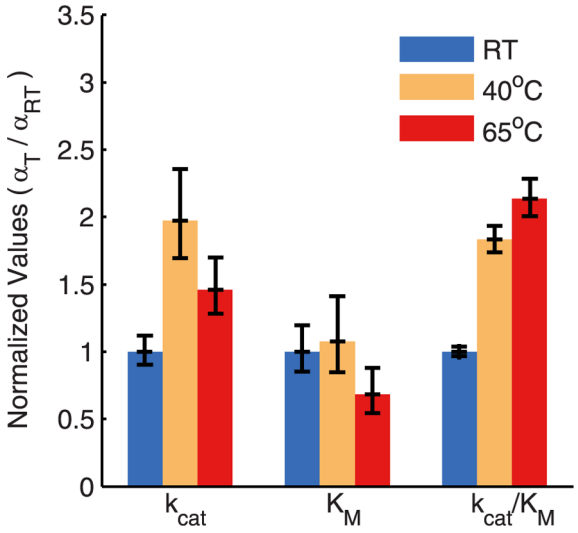

Figure 5. DDAH catalytic efficiency increases in higher temperatures. DDAH samples were solubilized in DMSO at the given temperatures and incubated for 30 min before substrate was added. After subtracting background activity of 25 μM $ZnSO_4$, each catalytic parameter (α_T) is determined by Lineweaver–Burk analysis and normalized to the room temperature value (α_{RT}). Error bars represent 95% confidence intervals.

close to the room temperature value, such that the overall catalytic efficiency increased with higher temperatures to twice that at room temperature. The stability of the M13 capsid structure therefore leads to a robust active site capable of catalysis at a wide range of functional temperatures.

DISCUSSION

In this study, we have developed a novel strategy for biocatalytic studies: the incorporation of an enzymatic motif into thermostable bacteriophage particles to yield versatile semisynthetic enzymes. The selected clone, DDAH, mimicked the active site of carbonic anhydrase in its distribution of polar and hydrophobic residues. The presence of nonpolar amino acids in active sites has long been known to be critical for efficient catalysis, hypothesized to reduce the conformational variability of charged coordinating residues and/or increase the surrounding local dielectric field.[47] Indeed, mutation of V_{i5} or W_{i7} to alanine significantly decreases the catalytic activity of DDAH, highlighting the important role these residues play in the clone's active site. The activity is contingent upon the quaternary structure of M13's coat proteins, as soluble peptides exhibited negligible activity. In addition, the complete inactivity of the Δ3H clone in water renders highly unlikely the possibility that measured catalysis is the result of contaminant *Escherichia coli* detritus from our bacteriophage purification protocols. pNPA hydrolysis, a useful representative reaction for enzymatic activity, will inform future engineering efforts toward more complex target reactions. The demonstrated display and organization of multiple metal-coordinating residues on all 2700 pVIII proteins is a novel capability and will allow for the coordination of other cofactors and replication of other enzymatic activities. While the aqueous catalytic efficiency remains substantially lower than that measured for wild-type bCAII, the activity is nonetheless comparable to *de novo* enzymes reported by Zastrow et al.[31] for the same pH, at pH 7.5, k_{cat}/K_M = 1.38 M^{-1} s^{-1} per three helices, and Patel et al.,[33] at pH 8, k_{cat}/K_M = 9.9 M^{-1} s^{-1} per four helices. Recent works by the Kuhlman group (k_{cat}/K_M at pH 7.5 = 90 M^{-1} s^{-1} for two zinc coordination sites) and Rufo et al. (at pH 8, k_{cat}/K_M = 62 M^{-1} s^{-1} per amyloid peptide) have made substantial improvements in rates for aqueous esterolysis and are informative for ongoing enzyme design, but neither approach demonstrates solvent/thermostable activity nor enables genetic screens.

The environmental robustness inherent to the M13 viral capsid is a key feature in its use as a biocatalytic platform. In particular, its compatibility with organic solvents and its thermostability are advantageous for numerous applications. Here, the stability of DDAH in DMSO allowed for the catalysis of substrates and reactions not practical in aqueous solutions, broadening the potential application space. The increase in activity observed in DMSO may be a result of conformational rigidity imparted by hydrophobic solvent interactions with pVIII N-terminal residues,[12] which lack known secondary structure in aqueous solutions. The well-characterized α-helix formed by pVIII is likely broken by the proline in position 6, resulting in an unknown conformation for the most N-terminal 10 residues. If these residues, which include our inserts, are more restrained conformationally in less polar solvents,[12] then this likely contributes substantially to the increase in catalytic activity observed. Additionally, as the M13 active site is relatively small, substrates may remain partially exposed to the surrounding solvent, in which case nonpolar solvents can increase activity.[48] In addition to DMSO, the phage is compatible with ethane diol (Supplementary Table 3), and other solvents will be characterized in future work. Given the number of important feed stocks and precursor compounds insoluble in water, such diverse solvent compatibility is of immense utility. Furthermore, the increasing catalytic efficiencies at raised temperatures makes M13 biocatalysts amenable to a wider range of reactions and reduced risks of bacterial contamination.

More broadly, M13's well-understood biology and dense display of peptides make it appealing for future development. The ease of bacteriophage amplification and purification allows for greater scalability of the catalysts compared to other enzymatic proteins, while pVIII's tightly packed, highly multivalent structure leads to higher numbers of reaction centers. With thousands of pVIII proteins per biomolecule, M13 can stably approach millimolar concentrations of active sites with or without immobilization. Moreover, the inherent inclusion of the bacteriophage genome with all progeny makes functional catalytic selections from diverse libraries possible, whereas traditional enzymes lack the requisite genotype–phenotype connection. Accordingly, future engineering of the bacteriophage will harness its high multivalency and genotype–phenotype linkage in conjunction with recent developments in high-throughput assays, such as microengraving and microemulsions,[49] to search a larger sequence space for active clones. M13 biology further allows for directed evolution and host rescue assays to rapidly select functional variants. M13's genome itself is highly engineered, with numerous restriction enzyme sites in the genes of its various coat proteins, such that complementary binding or catalytic functions can be incorporated at other positions on the bacteriophage capsid.

CONCLUSION

Broader biochemical toolkits and a greater understanding of biocatalysis are critical in order to meet accelerating society-wide demand for chemicals, food, and materials. Proteins offer enhanced performance, novel chemical activity, and greater

dx.doi.org/10.1021/ja506346f | J. Am. Chem. Soc. 2014, 136, 16508–16514

environmental compatibility with respect to prevalent inorganic catalysts. We have identified an M13 bacteriophage clone with novel catalytic properties and thermal stability, in the process demonstrating M13 to be a versatile, high-surface area platform for biocatalytic engineering. Future work will build on these results by expanding M13 bacteriophage library diversity, improving selection methodology, evolving clones toward unique reactions, and fabricating stable catalytic macrostructures.

■ ASSOCIATED CONTENT

Supporting Information

Experimental procedures, electron microscopy, and other supporting data. This material is available free of charge via the Internet at http://pubs.acs.org.

■ AUTHOR INFORMATION

Corresponding Author

belcher@mit.edu

Notes

The authors declare no competing financial interest.

■ ACKNOWLEDGMENTS

We thank Jacqueline Ohmura for the image in Supplementary Figure 4b as well as the Center for Materials Science and Engineering for access to transmission electron microscopy for both images in Supplementary Figure 4. Additionally, we would like to acknowledge the Swanson Biotechnology Core at the MIT Koch Institute for Integrative Cancer Research for bacteriophage DNA sequencing.

■ REFERENCES

(1) Koeller, K. M.; Wong, C. H. *Nature* **2001**, *409*, 232.
(2) Schmid, A.; Dordick, J. S.; Hauer, B.; Kiener, A.; Wubbolts, M.; Witholt, B. *Nature* **2001**, *409*, 258.
(3) Gotor-Fernández, V.; Brieva, R.; Gotor, V. *J. Mol. Catal. B* **2006**, *40*, 111.
(4) *The Application of Biotechnology to Industrial Sustainability - A Primer*; OECD Publishing: Paris, France, 2001.
(5) White, N. J. *Science* **2008**, *320*, 330.
(6) Schmidt-Dannert, C.; Umeno, D.; Arnold, F. H. *Nat. Biotechnol.* **2000**, *18*, 750.
(7) Arnold, F. H. *Nature* **2001**, *409*, 253.
(8) Joseph, B.; Ramteke, P. W.; Thomas, G. *Biotechnol. Adv.* **2008**, *26*, 457.
(9) Nielsen, J.; Fussenegger, M.; Keasling, J.; Lee, S. Y.; Liao, J. C.; Prather, K.; Palsson, B. *Nat. Chem. Biol.* **2014**, *10*, 319.
(10) Reetz, M. T. *J. Am. Chem. Soc.* **2013**, *135*, 12480.
(11) Kim, J.; Jia, H. F.; Wang, P. *Biotechnol. Adv.* **2006**, *24*, 296.
(12) Klibanov, A. M. *Nature* **2001**, *409*, 241.
(13) Serdakowski, A. L.; Dordick, J. S. *Trends Biotechnol.* **2008**, *26*, 48.
(14) Perry, L. J.; Wetzel, R. *Science* **1984**, *226*, 555.
(15) Zhou, Z.; Hartmann, M. *Chem. Soc. Rev.* **2013**, *42*, 3894.
(16) Bommarius, A. S.; Paye, M. F. *Chem. Soc. Rev.* **2013**, *42*, 6534.
(17) Rodrigues, R. C.; Berenguer-Murcia, A.; Fernandez-Lafuente, R. *Adv. Synth. Catal.* **2011**, *353*, 2216.
(18) Moore, J. C.; Arnold, F. H. *Nat. Biotechnol.* **1996**, *14*, 458.
(19) Lipovsek, D.; Antipov, E.; Armstrong, K. A.; Olsen, M. J.; Klibanov, A. M.; Tidor, B.; Wittrup, K. D. *Chem. Biol.* **2007**, *14*, 1176.
(20) Giger, L.; Caner, S.; Obexer, R.; Kast, P.; Baker, D.; Ban, N.; Hilvert, D. *Nat. Chem. Biol.* **2013**, *9*, 494.
(21) Turner, N. J. *Nat. Chem. Biol.* **2009**, *5*, 567.
(22) Jochens, H.; Stiba, K.; Savile, C.; Fujii, R.; Yu, J. G.; Gerassenkov, T.; Kazlauskas, R. J.; Bornscheuer, U. T. *Angew. Chem., Int. Ed.* **2009**, *48*, 3532.
(23) Coelho, P. S.; Wang, Z. J.; Ener, M. E.; Baril, S. A.; Kannan, A.; Arnold, F. H.; Brustad, E. M. *Nat. Chem. Biol.* **2013**, *9*, 485.
(24) Gatti-Lafranconi, P.; Hollfelder, F. *ChemBioChem* **2013**, *14*, 285.
(25) Regan, L.; Degrado, W. F. *Science* **1988**, *241*, 976.
(26) Kamtekar, S.; Schiffer, J. M.; Xiong, H. Y.; Babik, J. M.; Hecht, M. H. *Science* **1993**, *262*, 1680.
(27) Robertson, D. E.; Farid, R. S.; Moser, C. C.; Urbauer, J. L.; Mulholland, S. E.; Pidikiti, R.; Lear, J. D.; Wand, A. J.; Degrado, W. F.; Dutton, P. L. *Nature* **1994**, *368*, 425.
(28) Huang, S. S.; Koder, R. L.; Lewis, M.; Wand, A. J.; Dutton, P. L. *Proc. Natl. Acad. Sci. U.S.A.* **2004**, *101*, 5536.
(29) Farid, T. A.; Kodali, G.; Solomon, L. A.; Lichtenstein, B. R.; Sheehan, M. M.; Fry, B. A.; Bialas, C.; Ennist, N. M.; Siedlecki, J. A.; Zhao, Z. Y.; Stetz, M. A.; Valentine, K. G.; Anderson, J. L. R.; Wand, A. J.; Discher, B. M.; Moser, C. C.; Dutton, P. L. *Nat. Chem. Biol.* **2013**, *9*, 826.
(30) Das, A.; Hecht, M. H. *J. Inorg. Biochem.* **2007**, *101*, 1820.
(31) Zastrow, M. L.; Peacock, A. F. A.; Stuckey, J. A.; Pecoraro, V. L. *Nat. Chem.* **2012**, *4*, 118.
(32) Broo, K. S.; Brive, L.; Ahlberg, P.; Baltzer, L. *J. Am. Chem. Soc.* **1997**, *119*, 11362.
(33) Patel, S. C.; Bradley, L. H.; Jinadasa, S. P.; Hecht, M. H. *Protein Sci.* **2009**, *18*, 1388.
(34) Benson, D. E.; Wisz, M. S.; Liu, W. T.; Hellinga, H. W. *Biochemistry* **1998**, *37*, 7070.
(35) Bolon, D. N.; Mayo, S. L. *Proc. Natl. Acad. Sci. U.S.A.* **2001**, *98*, 14274.
(36) Rothlisberger, D.; Khersonsky, O.; Wollacott, A. M.; Jiang, L.; DeChancie, J.; Betker, J.; Gallaher, J. L.; Althoff, E. A.; Zanghellini, A.; Dym, O.; Albeck, S.; Houk, K. N.; Tawfik, D. S.; Baker, D. *Nature* **2008**, *453*, 190.
(37) Hunt, J. A.; Fierke, C. A. *J. Biol. Chem.* **1997**, *272*, 20364.
(38) Marvin, D. A.; Hale, R. D.; Nave, C.; Citterich, M. H. *J. Mol. Biol.* **1994**, *235*, 260.
(39) Marvin, D. A.; Welsh, L. C.; Symmons, M. F.; Scott, W. R. P.; Straus, S. K. *J. Mol. Biol.* **2006**, *355*, 294.
(40) Eriksson, A. E.; Jones, T. A.; Liljas, A. *Proteins* **1988**, *4*, 274.
(41) Pocker, Y.; Stone, J. T. *J. Am. Chem. Soc.* **1965**, *87*, 5497.
(42) Host, G.; Martensson, L. G.; Jonsson, B. H. *Biochim. Biophys. Acta, Proteins Proteomics* **2006**, *1764*, 1601.
(43) Nicoll, A. J.; Allemann, R. K. *Org. Biomol. Chem.* **2004**, *2*, 2175.
(44) Chen, L.; Bromberg, L.; Hatton, T. A.; Rutledge, G. C. *Polymer* **2007**, *48*, 4675.
(45) Savile, C. K.; Janey, J. M.; Mundorff, E. C.; Moore, J. C.; Tam, S.; Jarvis, W. R.; Colbeck, J. C.; Krebber, A.; Fleitz, F. J.; Brands, J.; Devine, P. N.; Huisman, G. W.; Hughes, G. J. *Science* **2010**, *329*, 305.
(46) Wheals, A. E.; Basso, L. C.; Alves, D. M. G.; Amorim, H. V. *Trends Biotechnol.* **1999**, *17*, 482.
(47) Yamashita, M. M.; Wesson, L.; Eisenman, G.; Eisenberg, D. *Proc. Natl. Acad. Sci. U.S.A.* **1990**, *87*, 5648.
(48) Gomez-Tagle, P.; Vargas-Zuniga, I.; Taran, O.; Yatsimirsky, A. K. *J. Org. Chem.* **2006**, *71*, 9713.
(49) Love, K. R.; Bagh, S.; Choi, J.; Love, J. C. *Trends Biotechnol.* **2013**, *31*, 16.